Journal of Materials Chemistry A

HIGHLIGHT

View Article Online
View Journal | View Issue

Cite this: J. Mater. Chem. A, 2023, 11, 10463

Emerging high entropy metal sulphides and phosphides for electrochemical water splitting

Ranjit Mohili,†[a] N. R. Hemanth,†[b] Haneul Jin,†[c] Kwangyeol Lee *[d] and Nitin Chaudhari *[a]

Received 30th December 2022
Accepted 1st March 2023

DOI: 10.1039/d2ta10081a

rsc.li/materials-a

Hydrogen is expected to be a major clean and renewable energy source in the coming decades. Numerous electrocatalysts, including noble metals, oxides, hydroxides, carbides, transition metal phosphides/sulfides, and graphene-based materials, have been studied to produce hydrogen efficiently. Nevertheless, the demand for electrocatalysts with desired catalytic activity and stability in the hydrogen evolution reaction and oxygen evolution reaction has been largely unmet. High-entropy metal sulfides/phosphides (HEMSs/Ps) are a new class of materials, in which at least five (or >5) different principal metal elements are deliberately incorporated into a homogeneous single-phase sulfide or phosphide structure and have received significant attention due to the highly active site densities and potential synergy between multiple elements toward electrocatalysis. Although limited examples are available for these emerging materials, recent studies have demonstrated the great potential of HEMSs/Ps in the energy material horizon. This highlight emphasizes the synthetic strategies, unique electrocatalytic properties, and challenges and perspectives of HEMS/P electrocatalysts.

1. Introduction

Hydrogen (H_2) is an ideal clean chemical–electrical energy conversion medium as it creates zero pollution. Currently, most of the H_2 is produced from the steam reforming process of fossil fuels and biomass,[1] which emits large amounts of the greenhouse gas carbon dioxide (CO_2). Electrochemically splitting water into H_2 and oxygen (O_2) is a clean and sustainable

[a]Advanced Hybrid Nanomaterial Laboratory, Department of Chemistry, School of Energy Technology, Pandit Deendayal Energy University, Gandhinagar, 382426, Gujarat, India. E-mail: nitin.chaudhari@sot.pdpu.ac.in

[b]Department of Materials Science and Engineering, University of Washington, Seattle, 98195, WA, USA

[c]Department of Energy and Materials Engineering, Dongguk University-Seoul, Seoul, 04620, Republic of Korea

[d]Department of Chemistry and Research Institute for Natural Sciences, Korea University, Seoul, 02841, Republic of Korea. E-mail: kylee1@korea.ac.kr

† These authors contributed equally to this work.

Professor Kwangyeol Lee obtained his PhD degree (1997) in Chemistry from the University of Illinois at Urbana-Champaign. After fulfilling his military obligation, he joined Korea University in 2003 as a chemistry faculty member, before being appointed as a professor. His current interests include the development of synthetic methodologies for nanoscale materials and the development of nanotechnologies to support the environment by creating sustainable energy sources.

Dr. Nitin Chaudhari is an Associate Professor at Pandit Deendayal Energy University, Gandhinagar, India. He received his PhD degree in Materials Science from Korea University, South Korea in 2013. He subsequently worked as a Research Professor at Myongji University and Korea University, South Korea from 2013 to 2019. Later, he joined Nexcoms Ltd. Co., South Korea as a Deputy Director before moving to India. His research interests include the design and development of active electrode materials such as porous carbons, nanocomposites, oxides, sulphides, hydroxides, 2D MXenes, and nanomaterials for energy storage and conversion devices.

technology for producing H_2 when coupled with electricity generated in sustainable fashions because the initial feedstocks are water molecules.[2,3] Water electrolysis is an energy-intensive process involving two half-reactions, namely hydrogen evolution reaction (HER) and oxygen evolution reaction (OER).[4–6] The free energy barrier associated with the two half-reactions needs to be lowered by using efficient electrocatalysts to achieve cost-effective water electrolysis.[2,7]

The relentless pursuit for efficient electrocatalysts has engendered various active materials such as Pt/C, Pd/C, MoS_2, and g-C_3N_4 for the HER, and IrO_2, layered double hydroxides (LDHs), and Ni_3S_2 for the OER, respectively.[2,7–13] Transition-metal phosphides (TMPs) have also been regarded as promising electrocatalysts for overall water splitting because of their high catalytic activity stemming from the distinctive charge states and high electrical conductivity.[5,14] The phosphorus (P) element in TMPs facilitates a proton transfer and influences the catalytic activity, with a higher degree of phosphidation increasing HER activity.[15] Also, the tuneable electronic structure of metal phosphides can be advantageously explored for their potential use as electrocatalysts.[16,17] However, a higher P atom content can also inhibit metal atom electron delocalization, thereby limiting catalytic activity.[18] On the other hand, transition metal sulfides (TMSs) – M_xS_y have recently been explored as electrocatalysts due to their good electrical conductivity and potentially good electrochemical activity.[4,16,19] However, M_xS_y often suffers from poor stability, including thermodynamic instability, structural and morphological deformation, and catalyst detachment from the substrate under highly oxidative electrochemical conditions.[18] In addition, the unary, binary, and ternary M_xS_y catalysts lack broad compositional tunability.[20] In this regard, significant efforts have to be made to improve the catalytic capabilities of TMPs and TMSs.

High-entropy metal sulfides (HEMSs) and high-entropy metal phosphides (HEMPs) are composed of at least five or more different metal elements that are selectively combined into homogeneous single-phase sulfide or phosphide structures.[17] In contrast to unary, binary, or ternary metal chalcogenides (low entropy systems), HEMSs and HEMPs with multiple metal elements can achieve excellent compositional tunability towards the optimal adsorption of reaction intermediates to further boost overall water electrolysis according to the Sabatier principle.[21] Such a transformation from metal salts to high-entropy metal sulfides/phosphides (HEMSs/Ps) can be completed within hundreds of milliseconds, depending on the heating and flow rates.[22] Similarly, various combinations are available for allowing the regulation of the electronic and geometric structures for optimized catalytic activity.[20,23] Also, the polyanionic nature of these compounds provides unique electronic states and surface structures that are different from the commonly used catalysts, thus holding good promise for fast kinetics as well as good stability. Moreover, employing appropriate quenching techniques can achieve HEMSs/Ps with desired electronic states.[23]

Although very few examples of HEMSs/Ps have been reported at the current stage, the prospect of wide structural and compositional diversity and novel material properties from the discovery of new material classes is worthy of close inspection. HEMSs/Ps have been formulated as spherical particles with hollow structures, which featured an abundance of active sites to drive an efficient HER process.[22,24] The polycationic and polyanionic nature of these particles embraces unique electronic states that allow a facile flow of electrons, which is difficult to obtain in commonly used oxide based catalysts.[22] Self-reconstruction during the anodic oxidation process also allows the conversion of sulfides to metal (oxy)hydroxides, which have been demonstrated to be the real active sites.[20] All the different transition metal elements in HEMSs/Ps have variable oxidation states that give water molecules and intermediates a wide range of active sites to dissociate into H_2 and O_2 at a very low overpotential. An appropriate stoichiometric tuning of the metal element ratio can achieve better stability and selectivity in catalytic reactions over commercial catalysts such as IrO_2 or Pt-based materials. Therefore, we believe a timely highlight of the current research status on HEMSs/Ps would greatly facilitate advances in non-precious metal catalysts for water electrolysis. In this highlight, a great emphasis would be placed on the appealing anion-dependent properties of HEMSs/Ps, which are greatly tunable to make HEMSs/Ps promising electrocatalyst materials for water splitting.

2. Classification of HEMSs and HEMPs

Since electrochemical water splitting occurs on the surface of the electrode, tuning the catalyst surface characteristics, such as the type of metals and anions, stoichiometry, and electronic structures, is essential. The anion species itself, in particular, is of paramount importance to the properties of HEMSs/Ps because it locates cations in the anion frameworks and shifts the electronic structures through electron donation from anion to cation species, which is different from those of the conventional metallic high entropy alloys. In this context, this article classifies HEMSs/Ps in terms of the number of anions per metal atom: monoanionic, dianionic, and polyanionic HEMSs/Ps.

2.1 Monoanionic sulphides/phosphides

Monoanionic sulfides/phosphides are the primary type of HEMS/P containing five or more metals and one type of anion; for example, NiCoFeMnCrP nanoparticles[17] have five metal atoms (Ni, Co, Fe, Mn and Cr) and one phosphorus(P) anion atom. Similarly, CoFeNiMnMoPi,[22] CoCrFeMnNiP,[25] and ZnCoCuInGaS[26] catalysts all belong to monoanionic sulphides/phosphides.

2.2 Dianionic sulphides/phosphides

HEMS/P compounds containing five or more metals and two anions, where both anions can be the same or different, are referred to as dianionic sulfides/phosphides, and $FeNiCoCrMnS_2$ with[20] MS_2 configuration has been reported.

2.3 Polyanionic sulfides/phosphides

Adding more anions to the dianionic type results in polyanionic sulfide/phosphide formation, which can change the electronic

properties on the surface and the entire material. For example, $Co_{0.6}(VMnNiZn)PS_3$ has displayed superior retention of its thermodynamic stability, morphology, phase singularity, and catalytic activity compared to monoanionic and dianionic sulfides/phosphides.[24] The optimized distribution of anions on different sites and the polyanions may help bind metal elements to retain the morphology and phase singularity.[24,27]

3. Synthesis of HEMS and HEMP nanostructures

In general, the synthesis of HEMSs/Ps requires a high-temperature environment to incorporate multiple metals into a solid solution uniformly. The stabilization of the high-entropy state is also crucial to the integrity of the single-phase structure with unique electronic states and surface structures. Since the solid solution phase can be divided into thermodynamically stable sub-phases during cooling times, thus far, very few HEMPs and HEMSs with single-phase structures have been reported in the literature. Nonetheless, the properties observed in HEMSs/Ps are different from those of low-entropy metal sulfides or phosphides. The uniformity of the precursor solution, decomposition temperature, flow rate, reaction time, and quenching have been the deciding factors for the successful synthesis of HEMSs/Ps. The following have been the developed synthetic approaches for HEMS/P preparation until now.

3.1 High-temperature approach

Various high-temperature methods such as nebulization fly-through, eutectic solvent, furnace pulse deposition, simultaneous multi-exchange pathway, and solvothermal autoclave have been adopted to synthesize high entropy metal sulfides/phosphides.[22–25] For example, the loading of $(CrMnFeCoNi)S_x$ HEMS nanoparticles on a carbon substrate (carbonized wood) was achieved *via* a pulse thermal decomposition route by dissolving required metal salt precursors (chloride, nitride acetate, phosphate, *etc.*) and thiourea at 1377 °C followed by a fast quenching (Fig. 1).[20] Pulse thermal decomposition uniformly disperses and stabilizes multiple metals in the sulfide structure and overcomes the immiscibility issue to produce nanoparticle size between 10 and 40 nm. The high-temperature fly-through approach was also used to prepare a HEPi catalyst (*i.e.*, CoFeNiMnMoPi).[22] The precursor metal salts and tri-octyl phosphonium oxide (TOPO) were homogeneously confined into aerosol droplets through atomization, which was then thermally decomposed to a metal oxide and phosphorus, respectively. Afterward, HEPi particles were formed *via* thermal treatment at higher temperatures and rapid quenching. This *in situ* phosphating method significantly decreases the reaction time compared to phosphating the metal oxide, which typically takes several hours. Rapid quenching was found essential to fabricating high-entropy materials; otherwise, there would be elemental segregation or phase separation to their thermodynamically stable forms.

The simple and scalable synthesis route can help discover a range of polyanionic materials. In an attempt to make low-cost HEMPs using earth-abundant metals and overcome incompatibility between different metals and non-metals, Lai *et al.* developed a sol–gel strategy.[17] Equimolar amounts of metal precursors were mixed with $NH_4H_2PO_4$ and $C_6H_8O_7.H_2O$ followed by refluxing to obtain a uniform sol, which was then converted to gel ash by drying. The gel ash was then converted into black-coloured powder by calcination in an inert atmosphere (Fig. 2). During the calcination process of unary phosphides to high entropy phosphides, the hexagonal crystal phase of the substance remained unchanged. The sol–gel followed by the calcination method gave HEMP nanoparticles with an average diameter of about 300 nm.

The high configurational entropy of the randomized elements drives the formation of high-entropy materials; therefore, high temperatures and quenching are crucial to their stabilization.[28] A solid-state reaction was also reported synthesizing high-entropy metal phosphorus trichalcogenides ($MPCh_3$).[27] The elemental powders were ground uniformly and sealed into quartz tubes under vacuum and

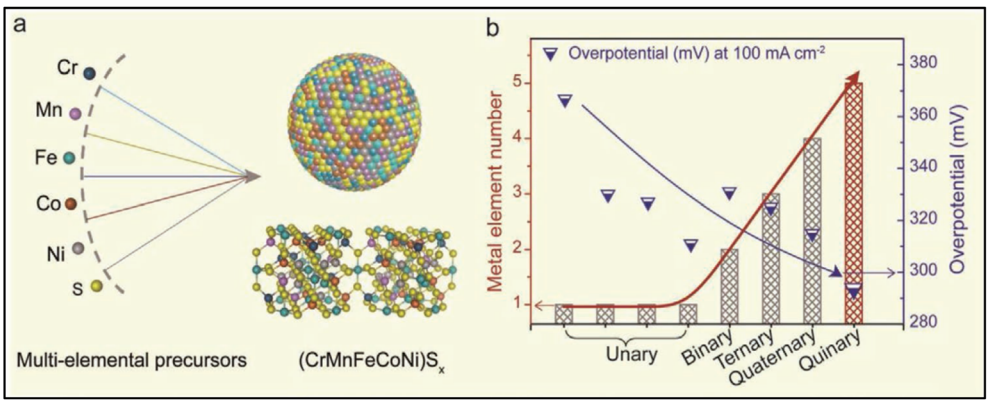

Fig. 1 Schematic demonstrating the structure of HEMS $(CrMnFeCoNi)S_x$ nanoparticles and their application as an OER catalyst. (a) Mixing immiscible metallic elements (*i.e.*, Cr, Mn, Fe, Co, and Ni) into a homogeneous and high-entropy sulfide nanoparticles. (b) Comparison of overpotentials and metal element numbers among unary, binary, ternary, and quaternary materials, and quinary HEMSs[23] (Copyright 2020, Wiley.).

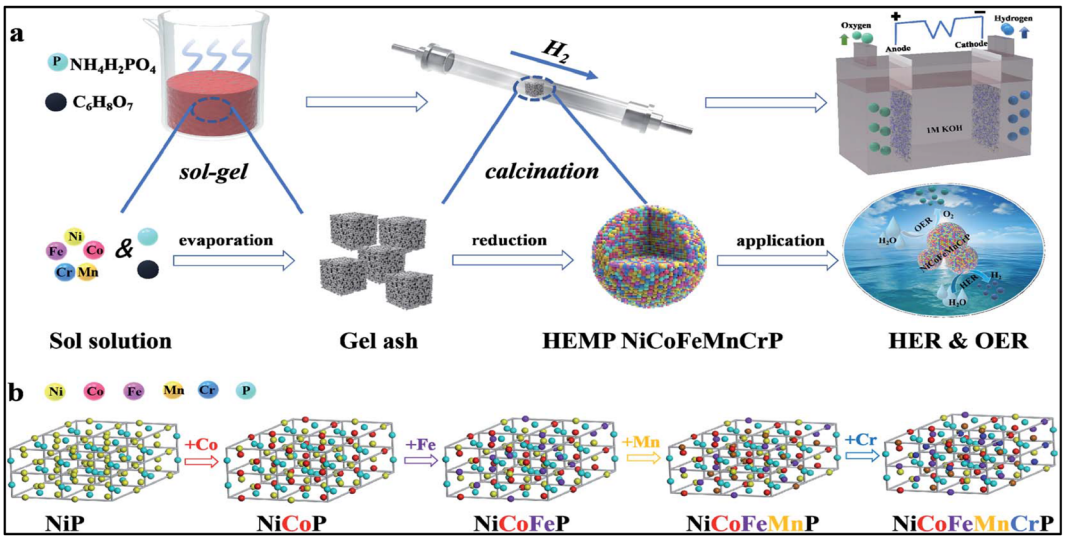

Fig. 2 (a) The synthesis process of HEMP NiCoFeMnCrP NPs for electrocatalytic water splitting through the sol–gel method and calcination reduction strategy; (b) the evolution of the crystal structures of NiP, NiCoP, NiCoFeP, NiCoFeMnP, and NiCoFeMnCrP NPs[17] (Copyright 2021, Royal Society of Chemistry.).

heated in a muffle furnace at 610 °C. The bulk products were ultrasonically exfoliated into high-entropy $MPCh_3$ nanosheets (NSs). Most of the metal phosphide synthesis processes use sodium hypophosphite, which releases toxic phosphine at high temperatures. However, Zhao *et al.* developed a non-toxic approach for preparing HEMPs using the eutectic solvent method.[25] First, a eutectic solvent was readily prepared by mixing equimolar amounts of metal chloride hydrates, tetrabutylphosphonium chloride (TBPC), and ethylene glycol (EG). The eutectic solvent has a melting point of 68 °C, lower than individual precursors, because of the hydrogen-bond networks. Subsequently, the eutectic solvent was thermally treated in an inert atmosphere to obtain a black powder of HEMP without any post-treatment steps. Another approach for low-temperature HEMS synthesis was reported by Xuyen *et al.*[20] High entropy $FeNiCoCrMnS_2$ particles, having a core–shell-like structure were first synthesized using a solvothermal approach at low temperatures. Micro-sized glycerate template particles containing metal ions were prepared first, and the template particles were sulfurized with thioacetamide, resulting in a quinary metal system $FeNiCoCrXS_2$ (X = Mn, Cu, Zn, or Al).

3.2 Low-temperature cation-exchange approach

Low-temperature synthesis of HEMSs/Ps was not reported, yet we will discuss a simultaneous exchange pathway in this section.[26] Firstly, colloidal roxbyite copper sulfide (CuS) nanoparticles were pre-treated in hexane. Appropriate volumes of $ZnCl_2$, $CoCl_2$, $InCl_3$, and $GaCl_3$ solutions were stirred in a round-bottom flask, and then benzyl ether, OLAM, and ODE were added and heated. Secondly, the sonicated suspension of CuS in TOP (Tri-octyl phosphine) was rapidly injected into the above reaction mixture. The reaction mixture was cooled and centrifuged using a mixture of IPA, acetone, and toluene. A red/brown single crystalline wurtzite-type Zn–Co–In–Ga–Cu sulfide product was then suspended in hexane.

3.3 Miscellaneous method

The dittmarite structure, named after the dittmarite NH_4-$MgPO_4 \cdot H_2O$ mineral, has gained interest in many fields because of its layered structure.[28] High entropy NH_4(-MnFeCoNiZn)PO_4 was prepared *via* a mechanochemistry-assisted hydrothermal method. The process involves equimolar mixtures of fine blended powders of $MnCl_2$, $FeSO_4$, $CoCl_2$, $NiCl_2$, and $ZnSO_4$ being poured into boiling $(NH_4)_2HPO_4$ solution under stirring. The resulting high entropy NH_4(-MnFeCoNiZn)PO_4 product possessed a single-crystalline phase.

4. Crystal structures and morphology of HEMSs/Ps

As the physical and chemical properties of HEMSs/Ps are related to their surface atom arrangements, delicate control of the crystal structures and morphology is essential for tuning the surface properties toward electrochemical applications. Temperature selection is particularly important because the material synthesis temperature determines the crystal phases and mixing of S and P anions. As shown in Table 1, HEMPs are based predominantly on hexagonal M_2P-based crystal structures, which are commonly observed phases for metal phosphide nanomaterials, regardless of the annealing temperatures (400 °C(ref. [25]) and 900 °C). In contrast, HEMSs showed diverse crystal structures of M_3S_4, M_9S_8, or MS_2 because a low temperature is required for solvothermal syntheses (150–180 °C). On the other hand, in the case of $Co_{0.6}$(VMnNiZn)PS_3, a polyanionic HEMS was obtained by long-term thermal annealing at a high temperature of 610 °C for 168 h.[24]

Table 1 Synthesis methods, structure, and application of the reported HEMS/P electrocatalyst

Sr. No.	HEMS/P electrocatalysts	Synthetic route	Morphology	Crystal system (structure)	Application	Overpotential (mV @ 10 mA cm^{-2})	Tafel slope (mV dec^{-1})	Ref.
1	CoFeNiMnMoPi	Nebulization fly-through	Hollow sphere	Cubic (rock salt-type MO)	OER	270	74	22
2	CoCrFeMnNiP	Eutectic solvent	Sheet	Hexagonal (M_2P)	HER	136	85.5	25
					OER	320	60.8	
3	$(CrMnFeCoNi)S_x$	Furnace pulse deposition	Sphere	Cubic (mixed; $M_3S_4 + M_9S_8$)	OER	295	66	23
4	ZnCoCuInGaS	Simultaneous multi-exchange pathway	Sphere	Hexagonal (Wurtzite-type MS)	—	—	—	26
5	$FeNiCoCrMnS_2$	Solvothermal autoclave method	Yolk–shell sponge	Cubic (pyrite; FeS_2)	OER	199	39.1	20
6	$Co(VMnNiZn)PS_3$	Muffle furnace	Sheet	Monoclinic	HER	65.9	65.5	24
7	NiCoFeMnCrP NPs	Sol–gel method	Sphere	Hexagonal (M_2P)	HER	220	94.5	17
					OER	270	52.5	

The Kirkendall effect is frequently encountered during anion exchange reactions, leading to hollow structures that might be useful for catalytic applications. However, in the cases where structural retention is needed, the presence of the Kirkendall effect is undesirable. To address this issue, Schaak *et al.* reported a shape-maintaining HEMS with a tunable metal/sulfur ratio through a cation exchange method in ZnCoCuInGaS nanoparticles.[26] The stoichiometric control could convert the Cu sites into Zn, Co, In, and Ga sites in $Cu_{1.81}S$ (roxbyite) nanospheres. The thermodynamic stability of ZnCoCuInGaS was tested by annealing it at 300 and 600 °C, and strong single-phase retention was obtained.

5. HEMSs/Ps for electrochemical water splitting

Electrochemical water splitting is an electricity-driven and electrode surface-confined reaction, and the subtle balance of the atomic configuration and electronic structure of catalysts directly affects the catalytic performance.[29] In practical applications, the surface atomic configuration of HEMSs and HEMPs is considered random; since over five atoms are inter-fused, a topological control of a specific atom is hardly achieved. According to the Sabatier principle, the adsorption and desorption energies of reactants (reaction intermediates) should be balanced for an efficient electrocatalyst.[4,30] The unique electronic structures stemming from the multimetallic alloys can still affect the electrocatalytic performances by optimizing surface electronic states, and the anion effects in the HEMSs/Ps can be categorized by the number of participating anions.[31,32] For example, in the case of HEMSs/Ps with five metal elements, the ratios of sulfur or phosphorus in total elements are varied as 20, 33 and 43% for monoanionic, dianionic, and trianionic HEMSs/Ps, respectively. It was also revealed that the anion prefers proton adsorption during the HER or OER to promote dehydrogenation from the reaction intermediates.[16,33–35] Especially for the OER, the surface atoms determine the structure of the *in situ* formed oxyhydroxide layer, which provides active sites for the OER, and thus, the stoichiometric control of HEMSs/Ps is vital for improvement in OER performances.

In the following sub-section, we discuss the performance of HEMS/P-based electrocatalysts, particularly in the electrochemical hydrogen evolution reaction (HER) and oxygen evolution reaction (OER), and highlight the effects of cations and anions on the electrochemical water splitting. The performance level of HES/P materials is depicted in Table 1.

5.1 HEMs with monoanionic S/P for electrochemical water splitting

Mu *et al.* reported quinary metal phosphide nanoparticles (CoCrMnFeNiP, high-entropy metal phosphide, HEMP) with a single crystalline phase based on the iron phosphide structure (Fig. 3a).[25] The electrochemical hydrogen and oxygen evolution abilities of the HEMP were compared with mono-metallic phosphides in 1.0 M KOH. The HEMP showed enhanced performances for both the HER and the OER (Fig. 3b). For the HER, the HEMP showed an overpotential of 136 mV, which was

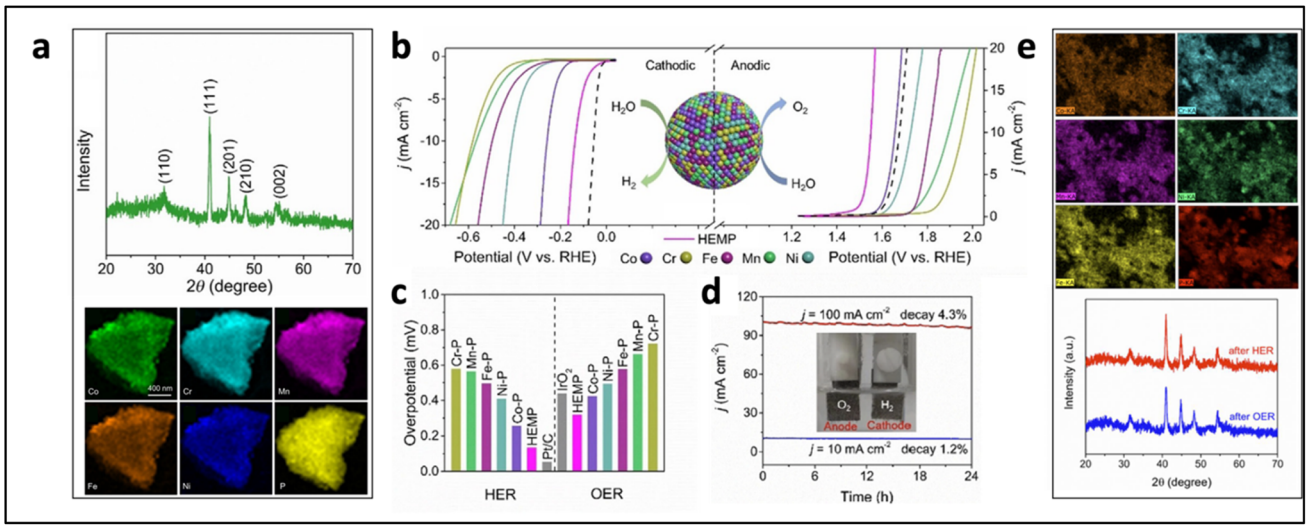

Fig. 3 (a) XRD analysis and elemental mapping images of CoCrMnFeNiP. (b) HER (left) and OER (right) performances of the HEMP electrocatalyst and their components. (c) Corresponding overpotential at a current density of 10 mA cm^{-2}. (d) Comparison of the polarization curves of the HEMP after 1000 cycles. (e) Elemental mapping images of each element and XRD analyses after the HER and OER[25] (Copyright 2020, Wiley.).

better than those of Co–P (258 mV), Cr–P (581 mV), Fe–P (497 mV), Mn–P (567 mV), and Ni–P (410 mV). Also, the HEMP reached 10 mA cm^{-2} at an overpotential of 320 mV, outperforming those of Co–P (427 mV), Cr–P (724 mV), Fe–P (580 mV), Mn–P (664 mV), and Ni–P (496 mV) as shown in Fig. 3c. The study reports a long-term stability test using the HEMP as both the cathode and the anode for 24 h. The HEMP-catalysed electrolytic cells demonstrated 1.2 and 4.3% decay of their current densities in 24 h at 10 and 100 mA cm^{-2}, respectively. The elemental mapping images and X-ray diffraction (XRD) analysis of the electrodes after the reaction showed stable physical properties of the HEMP against water splitting.

Likewise, Hu *et al.* reported a stoichiometry-controlled HES electrocatalyst with quinary ($(CrMnFeCoNi)S_x$), quaternary ($(MnFeCoNi)_9S_8$), ternary ($(FeCoNi)_9S_8$), binary ($(NiFe)_9S_8$), and unary metals (M_9S_8) through a pulse thermal decomposition (Fig. 4a).[23] Detailed physical analysis showed that cubic crystal structures ($Fm\bar{3}m$) were formed with the variable stoichiometry of quinary, quaternary, and ternary nanoparticles. The EDS quantified a ratio of 9 for metal elements and 8 for sulfur (47% sulfur in a total number of elements). The synthesized $CrMnFeCoNiS_x$ nanocatalysts outperformed the quaternary ($(MnFeCoNi)_9S_8$), ternary ($(FeCoNi)_9S_8$), binary ($(NiFe)_9S_8$), and unary nanocatalysts with the OER overpotential values of 295 mV at 100 mA cm^{-2} in

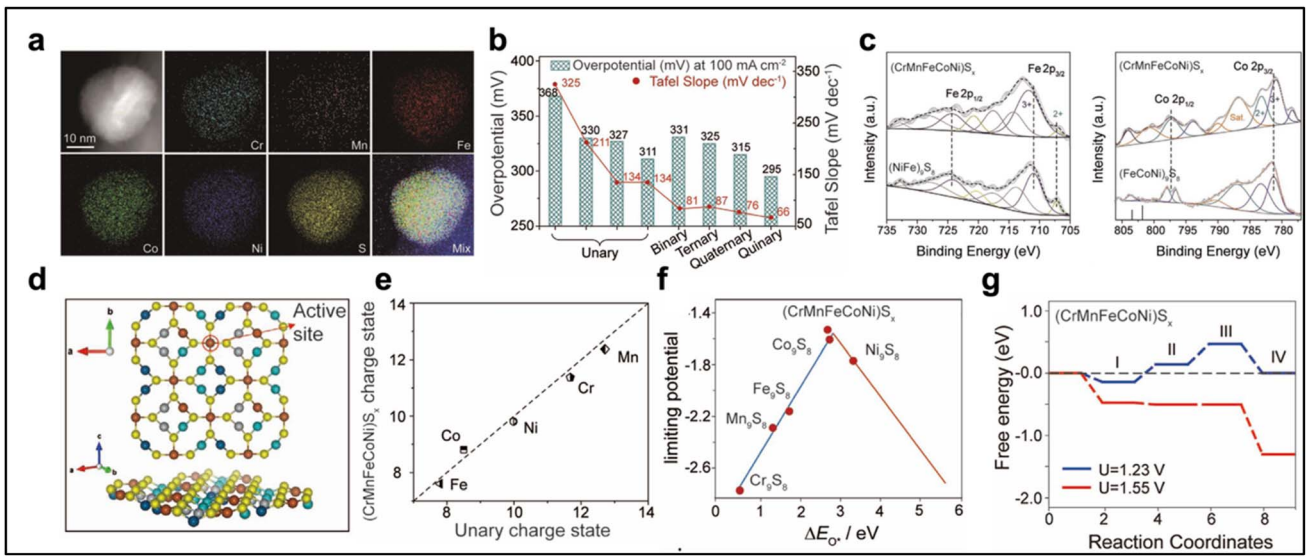

Fig. 4 (a) STEM and elemental mapping images of $(CrMnFeCoNi)S_x$. (b) Plots of overpotential and Tafel slope for unary, binary, ternary, quaternary, and quinary HESs. (c) XPS analyses at Fe 2p and Co 2p of $(CrMnFeCoNi)S_x$. (d) Schematics of the model of $Co_2Mn_1Fe_2Co_2Ni_2S_8$ and (e) its calculated relative charge states, (f) catalytic activity volcano plot, and (g) free energy diagrams in the oxygen evolution reaction[23] (Copyright 2021, Wiley.).

1 M KOH (Fig. 4b). Furthermore, the Tafel slope, which indicates an intrinsic activity of the catalyst, is lowered as the number of elements increases from 325 mV dec^{-1} (unary HES) to 66 mV dec^{-1} (quinary HES), implying that the intrinsic activity is the function of stoichiometry. XPS analysis revealed that the Co 2p3/2 peak moved toward the low binding energy region, while the Fe 2p3/2 peak shifted to the higher binding energy region (Fig. 4c). This result indicated electron donation from Fe to Co, which makes Co an electron-rich state in $CrMnFeCoNiS_x$. DFT calculation with the model of 2 : 1 : 2 : 2 : 2 for Cr/Mn/Fe/Co/Ni supported the electron-rich Co state and enhanced OER performances (Fig. 4d). The charge state differences between unary and quinary HESs were negative for Co (−0.31 e^-), while those for Fe (0.19 e^-), Ni (0.17 e^-), Cr (0.31 e^-), and Mn (0.34 e^-) are positive (Fig. 4e). The enhanced OER performances were compared using the plot of theoretical limiting potential as a function of O* adsorption energy (ΔE_{O^*}) and a volcano plot was obtained with the lowest potential of 1.55 V for $CrMnFeCoNiS_x$ (Fig. 4f). It was also revealed that the enhanced OER kinetics has originated from the lowered free energy values in the second ($\Delta G_{OOH^*} - \Delta G_{O^*}$) and third ($\Delta G_{O^*} - \Delta G_{OH^*}$) proton-electron transfer steps (Fig. 4g).

5.2 HEMs with dianionic S/P for electrochemical water splitting

Ting *et al.* reported yolk–shell structured high entropy sulfide catalysts using a two-step solvothermal method.[20] The quinary metal sulfide catalysts had a cubic pyrite structure with a yolk–shell morphology with crystalline and amorphous mixed phases on their surfaces (Fig. 5a). The quinary metal $FeNiCoCrMnS_2$ showed better performance as compared to quaternary, ternary, binary, and unary metal sulfides (Fig. 5b). Furthermore, the composition effect on OER activity was investigated by comparing the OER performances of Mn, Cu, Zn, or Al added $FeNiCoCrXS_2$ (Fig. 5c). LSV curves revealed that the overpotential of $FeNiCoCrXS_2$ at 1 A cm^{-2} changed in the order of Mn < Al < Cu < Zn. In particular, the OER performance of the Zn added HES was lower than that of the quaternary HES. *In situ* Raman spectroscopy was conducted to scrutinize the enhanced OER activity of $FeNiCoCrMnS_2$, which revealed the facile formation of M–OOH groups at an applied potential of 1.2 V for $FeNiCoCrMnS_2$, while higher potentials over 1.3 V were required to form the M–OOH groups for quaternary, ternary, and binary catalysts (Fig. 5d and e). The facilitated M–OOH formation was attributed to S^{2-} transition to SO_4^{2-} during the OER process by *ex situ* XPS analysis (Fig. 5f and g). The sulfur (S) 2p peaks at 163 and 164 eV relates to S^{2-} of metal disulfide, which gradually disappeared after a few minutes of reaction. Whereas the peak corresponding to sulphate component (SO_4^{2-}) located at 169 eV was maintained after 9 h of reaction. Also, for O 1s, OH^- and M–O peaks significantly grew after starting the OER, which indicated that most of the HES surface moieties were changed to M–OOH, coexisting with a small number of SO_4^{2-} groups.

5.3 HEMs with polyanionic S/P for electrochemical water splitting

High entropy phosphorus sulfides (HEPSs) contain both sulfur and phosphorus elements. Diverse stoichiometric combinations such as PS, PS_3, and PS_4 have been found, and PS_3 is

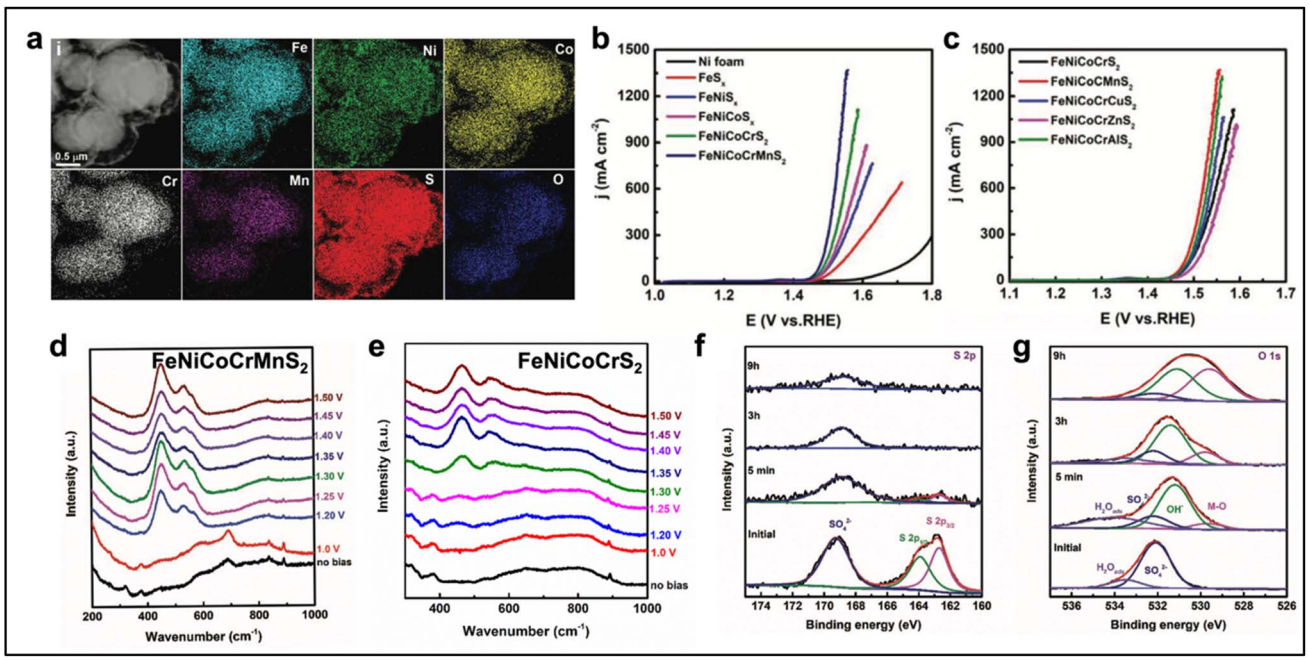

Fig. 5 (a) STEM and elemental mapping images of $FeNiCoCrMnS_2$ HES nanoparticles and (b) the OER performances of unary, binary, ternary, quaternary, and quinary HES nanocatalysts. (c) LSV polarization curves of $FeNiCoCrXS_2$ (X = Mn, Cu, Zn, and Al). (d and e) *In situ* Raman spectroscopy analyses of $FeNiCoCrMnS_2$ and $FeNiCoCrS_2$. (f and g) XPS analyses at S 2p and O 1s of $FeNiCoCrMnS_2$ [20] (Copyright 2021, Royal Society of Chemistry.).

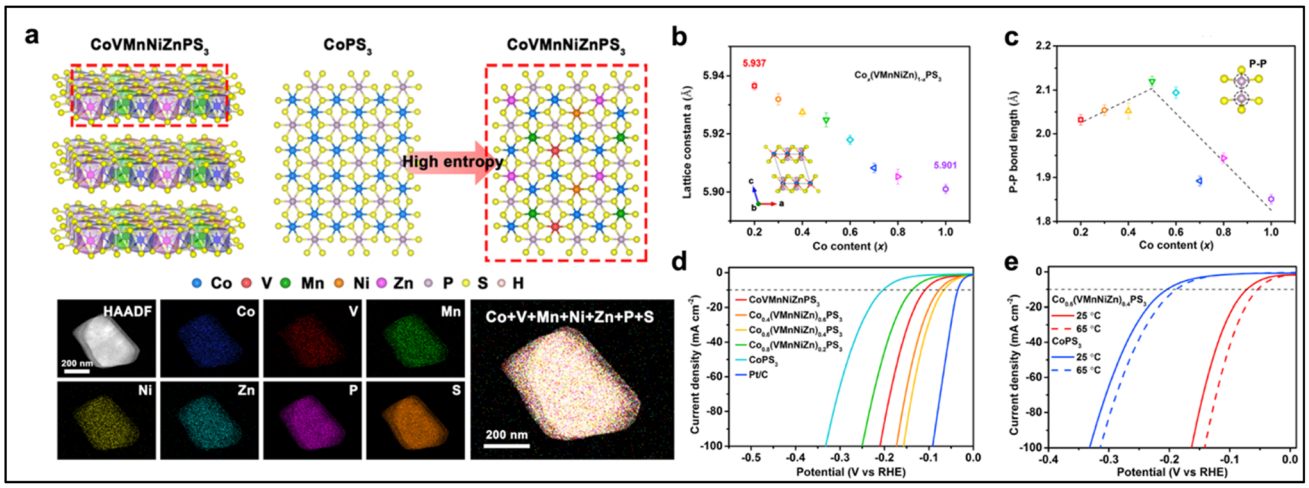

Fig. 6 (a) Schematics of a $CoVMnNiZnPS_3$ crystal (monoclinic structure (*C*2/*m*)) and the structural polymorphs of $CoPS_3$ and $CoVMnNiZnPS_3$. Plots of (b) the lattice constant *a* and (c) P–P bond length as a function of the ratio of Co(*x*). (d) Electrochemical HER performances of $CoVMnNiZnPS_3$ at different *x* ratios. (e) LSV curves of $CoVMnNiZnPS_3$ recorded at 25–65 °C[24] (Copyright 2022, American Chemical Society.).

a prominent composition based on CdI_2 and $CdCl_2$ crystal structures forming a $[P_2S_6]^{4-}$ complex with a 4+ formal oxidation state of phosphorus.[24] Therefore, metal species in the HEPS have an average oxidation state of 2+, which is different from widely known transition metal dichalcogenides (oxidation state of metal: 4+), pointing to a divergent behavior in electrocatalysis. Song *et al.* scrutinized the high entropy effects on hydrogen evolution activity through stoichiometric control of electrocatalytically active elements and others in a rigid anion structure of a 2-dimensional PS_3 nanosheet ($Co_x(VMnNiZn)_{1-x}PS_3$), where *x* varies from 0.2 to 1.0.[24] The XRD result revealed that more crystal distortion is applied to the low Co sample because of the random distribution of other elements (Fig. 6b). However, the longest P–P bond length was obtained in the $Co_{0.5}$ content sample ($Co_{0.5}(VMnNiZn)_{0.5}PS_3$), showing a volcano curve along the Co content (Fig. 6c). The OER performances of stoichiometry-controlled $Co_x(VMnNiZn)_{1-x}PS_3$ corresponded to the volcano P–P bond length curves revealing the best activity at $Co_{0.6}(VMnNiZn)_{0.4}PS_3$ in 1.0 M KOH (Fig. 6d). Also, $Co_{0.6}(VMnNiZn)_{0.4}PS_3$ maintained its activity for 12 h at 65 °C in 1 M KOH (Fig. 6e). The morphology and crystal structure of $Co_{0.6}(VMnNiZn)_{0.4}PS_3$ were preserved well after the stability test indicating the electrochemically stable nature of $Co_{0.6}(VMnNiZn)_{0.4}PS_3$. Furthermore, metal dissolution analysis by inductively coupled plasma mass spectroscopy revealed that only 0.37% of metals were dissolved after the stability test.

6. Summary and future direction

This highlight article elaborated on the synthesis and properties of HEMSs/Ps and their potential as electrocatalysts for electrochemical water splitting. The HEMS/P materials are classified depending on the number of anions: monoanionic, dianionic, and polyanionic sulfides and phosphides. After the introduction of the preparation methods, the electrochemical water-splitting behaviors of HEMSs/Ps were compared in terms of electronic effects. The notable improvement of the catalytic performances of HEMSs/Ps in electrochemical water splitting stems from (1) charge separation of cation and anion sites for water dissociation and proton transfer, respectively, (2) optimization of the electronic structures of the active elements by electron donation/withdrawal to/from nearby cations and anions, and (3) alloy effects enhancing their thermodynamic stability under electrochemical conditions. However, there are areas requiring further improvement for HEMS/P-based catalysts. Overall the electrical conductivities of metal sulfides and phosphides are 10^4–10^7 times lower than those of metals. To overcome the high resistance issue, robust synthetic protocols leading to small HEMS/P nanoparticles should be developed. Also, a HEMS/P with atomically controlled surface atom configuration has not been accomplished yet. The structural characterization of HEMSs/Ps with multiple metal cation types and random anion placements has been extremely difficult, requiring more thorough characterization of atom arrangement for HEMS/P materials by combining various advanced spectroscopic and microscopic tools such as TEM, XAS, PDF, and XRD.

The formation process of HEMSs/Ps has garnered substantial attention due to its potential far-reaching application impact. The utilization of *in situ* XRD technology in HEA research has shed light on the formation mechanism of high-entropy systems, providing a guide for developing advanced electrocatalysts.[36] It has been found that HEA possesses a face-centered cubic lattice structure, similar to metallic crystal structures. However, the formation process of the crystalline structures of phosphides and sulfides is more challenging to understand, thereby meriting further investigation. Hence, *in situ* observations of the HEMS/P formation process would be a highly sought research target.

The use of HEA as an electrocatalyst was proven successful only a few years ago.[37] Also, studies have revealed that the active sites in HEA catalysts are the most electronegative among the five elements.[38–41] On the other hand, HEMS/P materials are still

in their early stages as new electrocatalysts, with recent research primarily focusing on synthesis methods and component selection. The complex nature of the HEMS/P system, which consists of different transition metals with varying oxidation states, makes understanding the role of various active sites in electrode reactions a challenging task. The presence of anions and differing oxidation of metals in HEMSs/Ps adds to this complexity. Further research is necessary to achieve the optimal HER mechanism on the HEMS/P electrode surface through electron density redistribution or *in situ* operando characterization. Advancing this field of research will significantly enhance our understanding of HEMS/P electrocatalysts.

We believe that the unique physical and chemical nature of HEMSs/Ps would provide immense opportunities for developing non-precious metal-based electrocatalysts for water electrolysis and energy-related applications. In particular, multi-element HEMSs/Ps might eventually replace precious metal-based catalysts, completely solving the catalyst preparation cost issue. Although very few reports have dealt with the synthesis of HEMSs/Ps and their application in water splitting until now, we hope that this article provides significant insights to researchers in the fields of nanomaterials and electrochemistry to pursue practical materials of HEMSs/Ps for state-of-the-art water electrolysis systems.

Conflicts of interest

The authors declare that there are no competing interests.

Acknowledgements

This study was supported by the Department of Science and Technology (DST) under the joint India-Korea bilateral project (INT/Korea/P-52). This study was also supported by Pandit Deendayal Energy University (PDEU) under the Start-up grant ORSP/R&D/PDPU/2021/NC00/R0069. K. L. acknowledges funding from NRF-2019R1A6A1A11044070 and NRF-2020K1A3A1A19088726. Also, H. J. acknowledges funding from NRF-2022R1C1C2005786.

Notes and references

1 H. Jin, C. Guo, X. Liu, J. Liu, A. Vasileff, Y. Jiao, Y. Zheng and S. Z. Qiao, *Chem. Rev.*, 2018, **118**, 6337–6408.
2 J. Zhu, L. Hu, P. Zhao, L. Y. S. Lee and K.-Y. Wong, *Chem. Rev.*, 2020, **120**, 851–918.
3 *Nat. Energy*, 2016, **1**, 16127.
4 H. Jin, J. Joo, N. K. Chaudhari, S. Choi and K. Lee, *ChemElectroChem*, 2019, **6**, 3244–3253.
5 B. You and Y. Sun, *Acc. Chem. Res.*, 2018, **51**, 1571–1580.
6 I. Roger, M. A. Shipman and M. D. Symes, *Nat. Rev. Chem.*, 2017, **1**, 0003.
7 N. R. Hemanth, T. Kim, B. Kim, A. H. Jadhav, K. Lee and N. K. Chaudhari, *Mater. Chem. Front.*, 2021, **5**, 3298–3321.
8 W. Fu, H. He, Z. Zhang, C. Wu, X. Wang, H. Wang, Q. Zeng, L. Sun, X. Wang, J. Zhou, Q. Fu, P. Yu, Z. Shen, C. Jin, B. I. Yakobson and Z. Liu, *Nano Energy*, 2016, **27**, 44–50.
9 N. Cheng, S. Stambula, D. Wang, M. N. Banis, J. Liu, A. Riese, B. Xiao, R. Li, T.-K. Sham, L.-M. Liu, G. A. Botton and X. Sun, *Nat. Commun.*, 2016, **7**, 13638.
10 Y. Wu, G.-D. Li, Y. Liu, L. Yang, X. Lian, T. Asefa and X. Zou, *Adv. Funct. Mater.*, 2016, **26**, 4839–4847.
11 Y. Lee, J. Suntivich, K. J. May, E. E. Perry and Y. Shao-Horn, *J. Phys. Chem. Lett.*, 2012, **3**, 399–404.
12 Z. Cai, X. Bu, P. Wang, J. C. Ho, J. Yang and X. Wang, *J. Mater. Chem. A*, 2019, **7**, 5069–5089.
13 G. Ye, Y. Gong, J. Lin, B. Li, Y. He, S. T. Pantelides, W. Zhou, R. Vajtai and P. M. Ajayan, *Nano Lett.*, 2016, **16**, 1097–1103.
14 N. K. Chaudhari, P. Yu, B. Kim, K. Lee and J. Li, *Dalton Trans.*, 2018, **47**, 16011–16018.
15 Z. Pu, T. Liu, I. S. Amiinu, R. Cheng, P. Wang, C. Zhang, P. Ji, W. Hu, J. Liu and S. Mu, *Adv. Funct. Mater.*, 2020, **30**, 2004009.
16 J. Joo, T. Kim, J. Lee, S. Choi and K. Lee, *Adv. Mater.*, 2019, **31**, 1806682.
17 D. Lai, Q. Kang, F. Gao and Q. Lu, *J. Mater. Chem. A*, 2021, **9**, 17913–17922.
18 N. K. Chaudhari, H. Jin, B. Kim and K. Lee, *Nanoscale*, 2017, **9**, 12231–12247.
19 S. Anantharaj, S. R. Ede, K. Sakthikumar, K. Karthick, S. Mishra and S. Kundu, *ACS Catal.*, 2016, **6**, 8069–8097.
20 T. X. Nguyen, Y. H. Su, C. C. Lin and J. M. Ting, *Adv. Funct. Mater.*, 2021, **31**, 2106229.
21 Z. W. She, J. Kibsgaard, C. F. Dickens, I. Chorkendorff, J. K. Nørskov and T. F. Jaramillo, *Science*, 2017, 355.
22 H. Qiao, X. Wang, Q. Dong, H. Zheng, G. Chen, M. Hong, C.-P. Yang, M. Wu, K. He and L. Hu, *Nano Energy*, 2021, **86**, 106029.
23 M. Cui, C. Yang, B. Li, Q. Dong, M. Wu, S. Hwang, H. Xie, X. Wang, G. Wang and L. Hu, *Adv. Energy Mater.*, 2021, **11**, 2002887.
24 R. Wang, J. Huang, X. Zhang, J. Han, Z. Zhang, T. Gao, L. Xu, S. Liu, P. Xu and B. Song, *ACS Nano*, 2022, **16**, 3593–3603.
25 X. Zhao, Z. Xue, W. Chen, Y. Wang and T. Mu, *ChemSusChem*, 2020, **13**, 2038–2042.
26 C. R. McCormick and R. E. Schaak, *J. Am. Chem. Soc.*, 2021, **143**, 1017–1023.
27 R. Gusmão, Z. Sofer and M. Pumera, *Angew. Chem., Int. Ed.*, 2019, **58**, 9326–9337.
28 J. Fan, T. Wang, Y. Yuan, C. L. Do-Thanh, X. Suo, Z. Yang, H. Chen and S. Dai, *ACS Appl. Energy Mater.*, 2022, **5**, 3290–3297.
29 Y. Jiao, Y. Zheng, M. Jaroniec and S. Z. Qiao, *Chem. Soc. Rev.*, 2015, **44**, 2060–2086.
30 B. Zhang, X. Zheng, O. Voznyy, R. Comin, M. Bajdich, M. García-Melchor, L. Han, J. Xu, M. Liu, L. Zheng, F. P. García de Arquer, C. T. Dinh, F. Fan, M. Yuan, E. Yassitepe, N. Chen, T. Regier, P. Liu, Y. Li, P. de Luna, A. Janmohamed, H. L. Xin, H. Yang, A. Vojvodic and E. H. Sargent, *Science*, 2016, **352**, 333–337.
31 J. Park, T. Kwon, J. Kim, H. Jin, H. Y. Kim, B. Kim, S. H. Joo and K. Lee, *Chem. Soc. Rev.*, 2018, **47**, 8173–8202.
32 F.-Y. Chen, Z.-Y. Wu, Z. Adler and H. Wang, *Joule*, 2021, **5**, 1704–1731.

33 P. Liu and J. A. Rodriguez, *J. Am. Chem. Soc.*, 2005, **127**, 14871–14878.
34 O. Mabayoje, A. Shoola, B. R. Wygant and C. B. Mullins, *ACS Energy Lett.*, 2016, **1**, 195–201.
35 J. Ryu, N. Jung, J. H. Jang, H.-J. Kim and S. J. Yoo, *ACS Catal.*, 2015, **5**, 4066–4074.
36 H. Zhu, Z. Zhu, J. Hao, S. Sun, S. Lu, C. Wang, P. Ma, W. Dong and M. Du, *Chem. Eng. J.*, 2022, **431**, 133251.
37 Y. Yao, Z. Huang, P. Xie, S. D. Lacey, R. J. Jacob, H. Xie, F. Chen, A. Nie, T. Pu, M. Rehwoldt, D. Yu, M. R. Zachariah, C. Wang, R. Shahbazian-Yassar, J. Li and L. Hu, *Science*, 2018, **359**, 1489–1494.
38 J. Hao, Z. Zhuang, K. Cao, G. Gao, C. Wang, F. Lai, S. Lu, P. Ma, W. Dong, T. Liu, M. Du and H. Zhu, *Nat. Commun.*, 2022, **13**, 2662.
39 J. Hao, J. Li, Y. Zhu, S. Sun, S. Lu, M. Du and H. Zhu, *Chem. Commun.*, 2023, **59**, 772–775.
40 G. Feng, F. Ning, J. Song, H. Shang, K. Zhang, Z. Ding, P. Gao, W. Chu and D. Xia, *J. Am. Chem. Soc.*, 2021, **143**, 17117–17127.
41 H. Zhu, S. Sun, J. Hao, Z. Zhuang, S. Zhang, T. Wang, Q. Kang, S. Lu, X. Wang, F. Lai, T. Liu, G. Gao, M. Du and D. Wang, *Energy Environ. Sci.*, 2023, **16**, 619–628.